

## **International Journal of Materials and Product Technology**

ISSN online: 1741-5209 - ISSN print: 0268-1900

<https://www.inderscience.com/ijmpt>

---

### **Stiffness analysis of automobile aluminium alloy frame based on finite element model**

Bing Chen, Junfeng Wu, Lei Wang

**DOI:** [10.1504/IJMPT.2024.10062362](https://doi.org/10.1504/IJMPT.2024.10062362)

#### **Article History:**

Received:	13 July 2023
Last revised:	26 September 2023
Accepted:	06 November 2023
Published online:	22 February 2024

---

## Stiffness analysis of automobile aluminium alloy frame based on finite element model

---

Bing Chen\*, Junfeng Wu and Lei Wang

Faculty of Engineering,  
Huanghe Science and Technology University,  
Zhengzhou, 450063, China

and

Henan Engineering Research Center of Acoustic Meta-Structure,  
Huanghe Science and Technology University,  
Zhengzhou, 450063, China

Email: cb741236985@163.com

Email: tyc01062023@163.com

Email: wl830104@163.com

\*Corresponding author

**Abstract:** Existing frame stiffness analysis methods lack accuracy. Therefore, a finite element model-based stiffness analysis method for automobile aluminium alloy frames is proposed. The finite element model considers only the main structural components and simplifies their structures to improve calculation efficiency while meeting accuracy requirements. Various parts and components are modelled and assembled into the complete frame model, including the suspension system in the analysis. The model grid is divided, and additional mass and assembly mass are simplified as concentrated loads applied to supporting points, while the frame's own mass is simplified as uniformly distributed loads applied to nodes and elements. Bending stiffness and torsional stiffness are analysed to determine the stiffness characteristics of the aluminium alloy frame. Test results demonstrate that this design method enables accurate bending and torsional stiffness analysis of the aluminium alloy frame, with minimal errors, as low as  $2e+0.01 \text{ N}\cdot\text{m}^2$  and  $22 \text{ N}\cdot\text{m}/^\circ$ .

**Keywords:** finite element model; automobile aluminium alloy frame; stiffness analysis; bending stiffness; torsional stiffness.

**Reference** to this paper should be made as follows: Chen, B., Wu, J. and Wang, L. (2024) 'Stiffness analysis of automobile aluminium alloy frame based on finite element model', *Int. J. Materials and Product Technology*, Vol. 68, Nos. 1/2, pp.50–70.

**Biographical notes:** Bing Chen received his PhD in Science and Technology of Armament from Nanjing University of Science and Technology in 2007. He is currently a Lecturer in the Faculty of Engineering of Huanghe Science and Technology University. His research interests include structural mechanical simulation of complex loads, intelligent control and microgrid system simulation.

Junfeng Wu received his ME from North China University of Water Resources and Electric Power of Mechanical Design and Theory in 2008. He is currently an Associate Professor in the Faculty of Engineering of Huanghe Science and Technology University. His research interests include structural simulation, infinite element, CAD/CAD/CAE.

Lei Wang received his PhD in Control Science and Engineering from Air Force Engineering University in 2011. He is currently a Lecturer in the Faculty of Engineering of Huanghe Science and Technology University. His research interests include life prediction, industrial robot and intelligent control.

---

## **1 Introduction**

With the continuous development of economy, automobile has become one of the indispensable means of transportation. At present, the global car ownership has exceeded 1 billion and is still growing rapidly. The automobile plays an important role in people's life, national economy and national defence construction, and has a profound impact on people's lifestyle, values, learning methods and working methods. It can be said that the automobile has changed people's life and social form. In modern society, cars have become an indispensable part of people's life and production. However, in addition to making significant contributions to human civilisation, automobiles have also brought about a series of serious problems. The exhaust gas emitted by automobiles contains toxic gases such as hydrocarbons and carbon monoxide, which will cause certain harm to human health. It will also emit carbon dioxide, which will aggravate the greenhouse effect. In addition, the noise generated by automobiles will also cause environmental pollution. At present, the power source of automobiles is still oil, which is a non-renewable and limited resource. At present, saving energy and reducing environmental pollution have become the core issues that need to be solved urgently in the automotive industry. Therefore, in the new industrial revolution, the new energy vehicle industry has become an important reform direction, and many countries have introduced policies to support its development. In China, new energy vehicles have been identified as one of the key projects of emerging strategic industries. Among them, lightweight is the key form of new energy vehicles. According to relevant data, for every 10% reduction in vehicle mass, the energy consumption of the vehicle can be reduced by about 6–8%. In addition, for every 1,000 kg of curb weight reduction, the fuel consumption per 100 km of the vehicle can be reduced by 0.5 litre. On the premise of meeting various performance requirements of automobiles, as one of the three major assemblies, automobile body is becoming increasingly dominant. According to relevant statistical data, the frame accounts for a considerable proportion of the total vehicle mass, and the manufacturing cost accounts for a large proportion. Therefore, the realisation of lightweight body has a significant impact on reducing environmental pollution and improving fuel economy. At the same time, the development of lightweight automobile body is very helpful for the improvement of vehicle stability, comfort and power. Among them, the application of lightweight materials is a way that has been widely used. Aluminium alloys are favoured for their strong corrosion resistance, plasticity, high strength, low density and other advantages, and have a strong weight reduction effect. Combined with the structural optimisation design, the fuel economy of the vehicle can be greatly improved. In order to realise the optimisation design of aluminium alloy body structure, the stiffness analysis of aluminium alloy frame was carried out.

For the research of automobile frame stiffness analysis, the current research has achieved relatively rich research results. Doornebosch et al. (2021) put forward a finite

element modelling and stiffness analysis method of automobile frame based on Hyperworks. By comparing the test results with the simulation results, the accuracy is high, and the reliability of the analysis results can be verified by comparing the test results with the simulation results; efficiency. Using Hyperworks software for modelling and analysis can improve the efficiency of analysis. However, the possible disadvantage of this method is that it may be limited in modelling and analysis of complex frame structures. Stefenon et al. (2022) proposed a frame stiffness analysis method based on tube combined structure and finite element calculation plate, and proposed corresponding improvement design suggestions for the actual structure of the motorcycle according to the research results, which can put forward improvement design suggestions for the actual structure of the motorcycle and help optimise the stiffness performance of the frame. However, the possible disadvantage of this method is that the modelling and analysis process may be relatively complex, requiring a high level of technology and expertise. Sharma et al. (2021) proposed an analysis method of automobile frame stiffness based on ANSYS. The stress and torsional deformation of the frame were obtained through a series of steps such as modelling and solving, which provided a basis for the optimal design of the frame. The stress and torsional transformation of the frame were obtained through modelling and solving, which provided a basis for the optimal design. However, the possible disadvantage of this method is that it requires a long calculation time, and it may face certain challenges for the modelling and analysis of complex frame structures.

To solve the problems of the above methods, a stiffness analysis of automotive aluminium alloy frames based on finite element models is proposed.

## **2 Stiffness analysis of automobile aluminium alloy frame**

### *2.1 Finite element part model construction*

The stiffness analysis of automotive aluminium alloy frames based on finite element models has advantages such as high accuracy, fast iteration, cost-effectiveness, and flexibility. It can model local details of the frame, consider various complex factors, and provide high accuracy. At the same time, it can also be quickly iterated and optimised by adjusting model parameters or design schemes, saving costs and time. In addition, finite element analysis can also simulate different types of load conditions and comprehensively evaluate the stiffness performance of the frame. In summary, this analysis method can help optimise frame design and improve the performance and reliability of the entire vehicle. In view of the complexity of the automobile frame structure, the steps to build its finite element model are very tedious, and the structure is too refined not only has a huge workload, but also affects the calculation results. Therefore, in the case of meeting the accuracy requirements, only its main structure is considered, and its main structure is properly simplified to implement the construction of the automobile aluminium alloy frame finite element model. When establishing a finite element model of an automotive aluminium alloy frame, the idea of appropriately simplifying the main structure is to improve computational efficiency and simplify the model, while retaining critical stiffness and load transfer paths. This can be achieved by decomposing according to the structural hierarchy, simplifying material descriptions, selectively applying constraints, and ignoring details with less impact. However, when

simplifying the model, it is necessary to ensure accurate modelling of key characteristics to ensure the reliability of the results. Which simplification strategies to choose should be based on experience and engineering judgement, and strike a balance between accuracy and model complexity.

The principle of simplifying the main structure of the frame is to implement necessary and appropriate simplification on the premise of fully reflecting the actual structural mechanical properties of the automobile aluminium alloy frame. Through stiffness analysis, small size structures that have no effect on the overall stiffness, such as flanging, reinforcement, holes and openings, can be ignored. At the same time, the fillet considered from the angle of manufacturing and installation is directly simplified to a right angle. In addition, features that have no effect on the section characteristics, such as bolt holes, steps and grooves, can also be ignored.

The modelling method adopted is to first build the models of the parts of the aluminium alloy frame of the automobile, then assemble the parts, and finally complete the construction of the finite element model of the aluminium alloy frame of the automobile. The modelling software selected is ANSYS.

Define the material properties of the aluminium frame. The main material parameters of aluminium alloy frame are shown in Table 1.

**Table 1** Main material parameters of aluminium alloy frame

<i>S/N</i>	<i>Project</i>	<i>Parameter</i>	<i>Unit</i>
1	Material science	Al	-
2	Poisson's ratio	0.5	-
3	Modulus of elasticity	226,850	Mpa
4	Density	$8.1 \times 10^6$	kg/mm <sup>3</sup>
5	Tensile strength	500~620	Mpa
6	Yield stress	350	Mpa

The material parameters of bolts and other parts are shown in Table 2.

**Table 2** Material parameters of small parts such as bolts

<i>S/N</i>	<i>Project</i>	<i>Parameter</i>	<i>Unit</i>
1	Material Science	40Cr	-
2	Poisson's ratio	0.4	-
3	Modulus of elasticity	2.11E+11	Mpa
4	density	8,500	kg/mm <sup>3</sup>
5	tensile strength	520	Mpa
6	Yield stress	780	Mpa

In the construction of each part model, the model of the load-bearing part, namely the longitudinal beam model, is first constructed.

The bending stress of the longitudinal beam shall be calculated after the slot structure is selected, and the positions of the fixing holes of the frame assembly, the fixing connection holes of the relevant grouped supports, the fixing holes of the pipe harness, the process holes, the fixing holes of the pipe harness, and the connecting holes of the

frame and the relevant parts and devices are determined. The calculation process is as follows:

- 1 Calculate the support reaction force based on the force balance equation  $D_1$  and  $D_2$ .
- 2 The bending moment equation and shear force equation of longitudinal beam are obtained by singular function method.
- 3 Support reaction force  $D_1$  and  $D_2$  substitute into the bending moment equation and shear force equation of the longitudinal beam to obtain the maximum bending moment of the longitudinal beam  $E_{\max}$ .
- 4 Calculate the maximum bending moment of longitudinal beam under dynamic load  $E_{\max}'$ , the calculation formula is as follows:

$$E_{\max}' = hd_k E_{\max} \quad (1)$$

In formula (1),  $d_k$  is the dynamic load factor;  $h$  is the fatigue safety factor (Goswami et al., 2021).

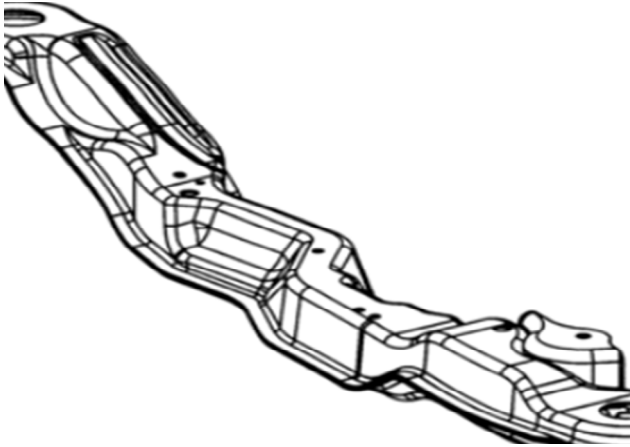
- 5 Calculate the bending stress of the longitudinal beam as follows:

$$P_W = \frac{E_{\max}'}{R} \quad (2)$$

In formula (2),  $R$  refers to the elastic modulus of the material.

According to the calculation results, RBE2 rigid beam element is used to simulate, and two longitudinal beam models are constructed. The simulation results of longitudinal beam model are shown in Figure 1.

**Figure 1** Simulation results of longitudinal beam model



Then, seven beam models are constructed, and the selected section shape is I-shaped structure, and the connection mode between them and the longitudinal beam is set as shown in Table 3.

Calculate the length of the leaf spring between beams, and the calculation formula is as follows:

$$V = 0.30 \times Z \quad (3)$$

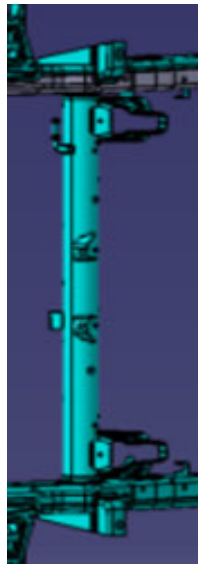
In equation (3),  $Z$  refers to the wheelbase.

Use the mpc184 rigid beam unit to build the beam model, as shown in Figure 2.

**Table 3** Connection mode of cross beam and longitudinal beam

<i>S/N</i>	<i>Beam name</i>	<i>Shape</i>	<i>Connection mode</i>
1	A crossbeam	U-shaped	Riveting with longitudinal beam wing surface
2	Second cross beam	U-shaped	Riveting with longitudinal beam wing surface
3	Three crossbeams	U-shaped	Riveting with longitudinal beam wing surface
4	Four crossbeams	Duckbill	Riveting with longitudinal beam wing surface
5	Five crossbeams	U-shaped	Riveting with longitudinal beam wing surface
6	Six crossbeams	U-shaped	Rivet the longitudinal beam wing surface with the connecting plate
7	VII crossbeam	U-shaped	Rivet the longitudinal beam wing surface with the connecting plate

**Figure 2** Beam model (see online version for colours)

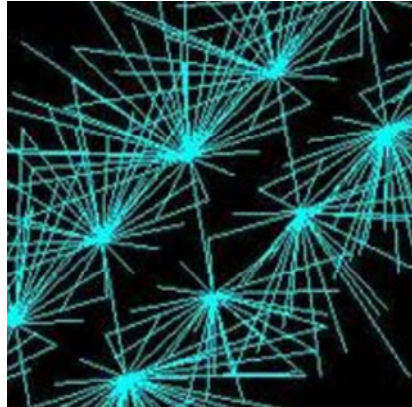


According to the calculation results and connection mode, add TYPE13 spring unit to build the finite element model frame of automobile aluminium alloy frame (Li et al., 2021).

## 2.2 Finite element overall model construction

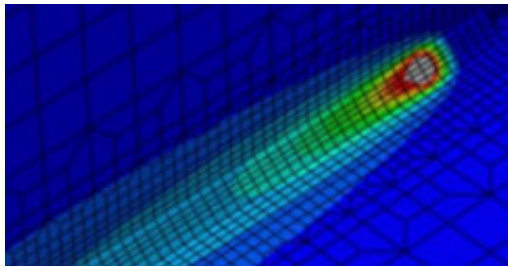
After the completion of the construction of the model frame of each part of the automobile aluminium frame, it is necessary to accurately simulate various connections to accurately transfer torque and force. The connection between non-main bearing parts and small parts mainly adopts spot welding, as shown in Figure 3.

**Figure 3** Spot welding method (see online version for colours)



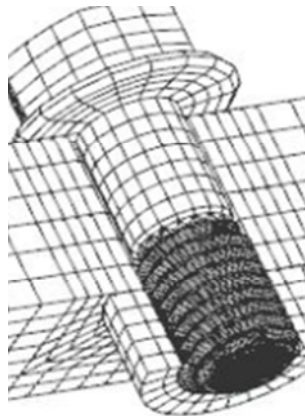
The cross beam and the longitudinal beam are connected by welds, as shown in Figure 4.

**Figure 4** Weld connection (see online version for colours)



The bolted connection adopts fixed multi-point constraint, as shown in Figure 5 (Depalo et al., 2022).

**Figure 5** Bolt connection mode



When constructing the solder joint element, it is necessary to ensure that the positions of the two nodes are relatively close, and if necessary, the positions of the nodes need to be adjusted to ensure the distance between the solder joints. The welding element shall also be perpendicular to the plane where the node is located, so as to make it consistent with the strength and stiffness of the actual welding point to the greatest extent.

After completing the construction of the frame model, it is also necessary to put the suspension system into the analysis category, that is, to implement reasonable simulation for the suspension. The front suspension studied is a double wishbone torsion bar spring independent suspension. Since the model is built to implement stiffness analysis, the torsional stiffness of torsion bar spring (Sayed and El-Sayed, 2022) is replaced by the linear stiffness method of suspension. The simulation method used is as follows: calculate the linear stiffness of the suspension using the corresponding geometric dimensions of the double wishbone and the actual torsional stiffness of the torsion bar spring, then assign the suspension linear stiffness value to the equivalent coil spring, and simulate the entire double wishbone suspension using the equivalent coil spring and the rigid beam.

The calculation formula of suspension line stiffness is as follows:

$$H = 2l_1 \left[ \frac{f}{z \cdot r - e \cdot (z - g)} \right]^2 \quad (4)$$

In equation (4),  $l_1$  is the stiffness of the torsion bar spring;  $f$  is the diameter of the torsion bar spring;  $z$  refers to the horizontal distance between the swing centre point of the lower control arm and the centre point of the wheel;  $r$  refers to the space distance from the left point of the lower arm to the left point of the upper arm;  $g$  refers to the space distance from the theoretical swing centre point of the upper arm to the left point of the lower arm.

The formula for calculating the stiffness of one side line of suspension is as follows:

$$H' = \frac{H}{2} \quad (5)$$

The COMBIN14 spring unit and MPC184 rigid beam unit are used to simulate the front suspension, the rigid beam is used to connect the two supports of the cross arm, and then the equivalent spiral spring is connected at the corresponding position of the front axle, with the rigidity of  $H$ , the length is the vertical distance from the front wheel central axis to the centre hole of the support, and the support hole and the rigid beam use multi-point constraints (Liu et al., 2022).

It is also necessary to simulate the rear suspension. The leaf spring dependent suspension is used, and the combination of rigid beam unit and spring unit is used to simulate. According to the stiffness of leaf spring  $B_0$  horizontal distance from the lower fulcrum of the spring to the front lifting lug  $A$  and the horizontal distance from the lower fulcrum of the spring to the rear lifting lug  $B$  the stiffness of two equivalent springs is calculated respectively, and the calculation formula is as follows:

$$L_0 = \frac{BB_0}{A+B} \quad (6)$$

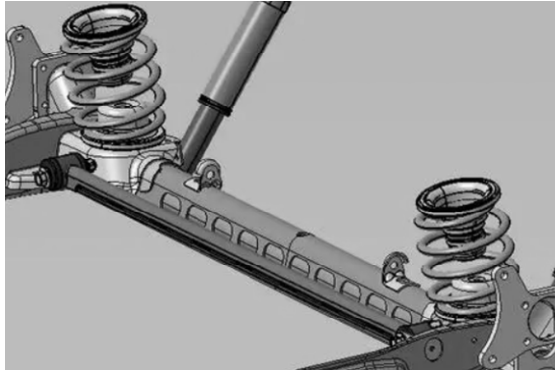
In formula (6),  $L_0$  refers to the stiffness of the left equivalent spring.

$$R_0 = \frac{AB_0}{A+B} \tag{7}$$

In equation (7),  $R_0$  refers to the stiffness of the right equivalent spring.

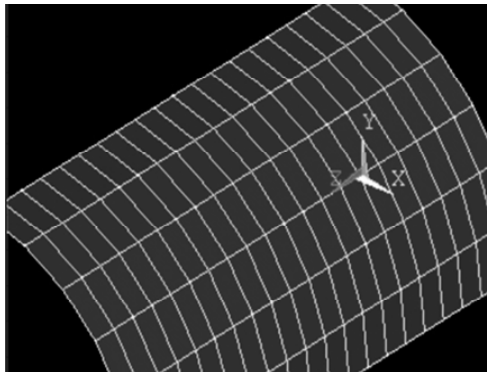
According to the calculation data, the finite element model of the rear suspension is built through MPC184 rigid connection unit and COMBIN4 spring unit. The spring unit is mainly used for the connection between the lifting lug and the leaf spring, and the rigid connection unit is mainly used for the connection between the spring units and between the two lifting lugs and the workshop, as shown in Figure 6 (Zhan et al., 2022).

**Figure 6** Finite element model of rear suspension

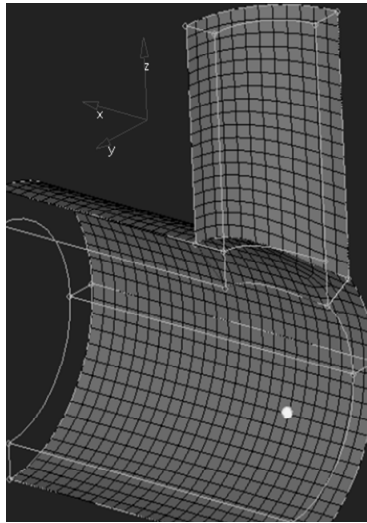


Since most of the structures in the aluminium alloy frame are thin-walled parts, in order to ensure the analysis accuracy, SHELL63 elastic shell element is used to implement the finite element network division of the main parts. The geometry and coordinate system of SHELL63 are shown in Figure 7.

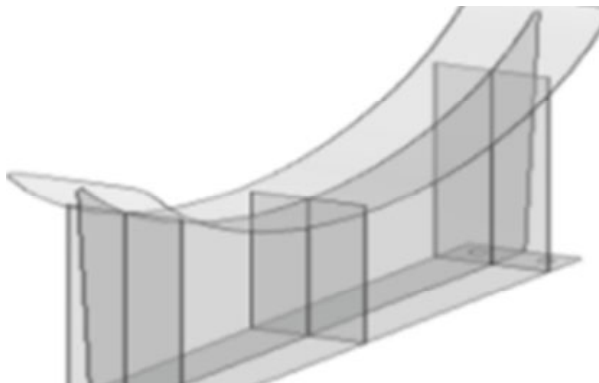
**Figure 7** Geometric shape and coordinate system of SHELL63



For the front connecting support part between the longitudinal beam and the double cross arm, it is impossible to divide it with SHELL63 elastic shell unit, so SOLID185 unit is selected for division. The geometry and coordinate system of SHELL63 are shown in Figure 8 (Jaafari et al., 2022).

**Figure 8** Geometric shape and coordinate system of SHELL63

Most parts of the automobile aluminium alloy frame are connected and welded by stamping thin plates through bolts. Therefore, after the shell element is selected for mesh generation, the middle surface of each part is extracted, and then the mesh generation is continued through the face element, and the part thickness is input when setting the material properties. This method can not only improve the grid quality and ensure the calculation progress, but also reduce the number of cells and ensure the calculation speed. The geometric figure after extracting the midplane is shown in Figure 9.

**Figure 9** Geometry after extracting the middle surface

In order to obtain the optimal grid quality, the grid division is carried out according to the parameters in Table 4 (Ci et al., 2022).

After the division, the grid quality needs to be reviewed. When there are substandard areas, they need to be adjusted manually.

**Table 4** Grid division parameters

<i>S/N</i>	<i>Project</i>	<i>Parameter</i>
1	Penalty value	0
2	Minimum side length	8
3	Maximum side length	16
4	Aspect ratio	3
5	Warpage	6
6	Maximum internal angle of quadrilateral	120
7	Minimum internal angle of quadrilateral	40
8	Maximum internal angle of triangle	130
9	Minimum internal angle of triangle	30
10	Twist	50
11	Jacobi	0.65
12	Chord difference	0.85
13	Triangle Percentage	9.50

### 2.3 Adding loads

When driving or stationary, the vehicle will be subject to multiple loads. After building the finite element model of the aluminium alloy frame of the vehicle, the load needs to be properly treated and applied to nodes and elements (Hajibabazadeh et al., 2021). When adding loads, the additional mass and the mass of each assembly are simplified as the concentrated load of the corresponding supporting point, and the mass of the aluminium alloy frame itself is simplified as the uniform load. The specific load addition is shown in Table 5.

**Table 5** Load addition

<i>Assembly</i>	<i>Quality</i>	<i>X coordinate corresponding to the point where each assembly is connected to the support</i>		<i>Position coordinates of assembly centroids in aluminium alloy frame coordinates</i>		
		<i>X1 (mm)</i>	<i>X2 (mm)</i>	<i>X (mm)</i>	<i>Y (mm)</i>	<i>Z (mm)</i>
Cab assembly	1,050	-1,580	1,050	-620	0	1,100
Aluminium alloy frame self-mass assembly	13,500	2,600	2,600	3,220	0	560
Engine clutch assembly	1,250	-650	852	750	0	-120

After the load is added, the finite element model of the aluminium frame is completely completed.

### 2.4 Stiffness analysis

The stiffness analysis of aluminium alloy frame finite element model is carried out from two aspects, namely bending stiffness analysis and torsional stiffness analysis.

In the bending stiffness analysis, a constraint is imposed on the position of the coil spring before the installation of the finite element model, so that it can only rotate around the Y axis, and a constraint is imposed on the rear suspension, retaining the RY and UX degrees of freedom, and the entire model is converted into a simply supported beam for calculation (Witkowski et al., 2022). Apply the concentrated force along the negative direction of the Z axis at the centre of the two constraints, and calculate the corresponding maximum displacement of the entire frame along the Z direction.

According to the bending stiffness calculation formula of the beam in the mechanics of materials, the bending stiffness calculation formula of the aluminium alloy frame model is obtained, as follows:

$$G = \frac{\alpha^2}{48} \times \frac{Q}{j} \quad (8)$$

In equation (8),  $\alpha$  refers to the distance between two loading points;  $j$  is the deflection of the loading point;  $Q$  refers to the loading force (De-La-Colina et al., 2021).

Since the rear suspension in the finite element model of the aluminium alloy frame is a leaf spring, the constraints on the rear suspension can be divided into three situations, that is, the constraints can be applied at three places, namely the front lifting lug of the leaf spring, the rear lifting lug of the leaf spring, and the support between the two, and the stiffness analysis (Saidou et al., 2021) can be carried out under three situations respectively.

- The first working condition: the constraint is imposed on the front lifting lug

At this time, the loading point is taken above the floor, the loading point is connected to 36 nodes on the adjacent floor, and a force of 4,000 N is applied in the left direction along the negative Z direction to obtain the deformation of the aluminium alloy frame, and the stiffness analysis is performed on it.

- The second working condition: the constraint is applied at the rear lifting lug

At this time, the loading point is taken above the floor, the loading point is connected to 36 nodes on the adjacent floor, and 4,000 N force is applied in the right direction along the negative Z direction to obtain the deformation of the aluminium alloy frame, and the stiffness analysis is performed on it.

- The third condition: constraint is imposed on the support between them

At this time, the loading point is taken above the floor, the loading point is connected to 36 nodes on the adjacent floor, and 4,000 N force is applied in the left and right directions along the negative Z direction respectively to obtain the deformation of the aluminium alloy frame, and the stiffness analysis (De et al., 2021) is performed on it.

Then the torsional stiffness analysis is carried out. In the analysis, the position of the coil spring is constrained before the installation of the finite element model, so that it can only rotate around the X axis, and the corresponding Z-direction translational degrees of freedom of the middle points of the left and right longitudinal beams are constrained, so as to achieve the restriction of the frame gravity caused by gravity.

Apply a pair of equal size and opposite direction in the Z direction at the front and rear lifting lugs of the rear suspension to make the aluminium alloy frame model undergo forced torsional deformation (Doornebosch et al., 2021). The torsional angle of the frame around the X axis is obtained by measuring the displacement at the bottom of the longitudinal beam in the same plane of Z direction and torque to obtain its torsional stiffness. The specific formula is as follows:

$$O = \frac{\varepsilon \cdot \beta \cdot \pi}{\arcsin\left(\frac{A_1 - A_2}{\beta}\right) \times 180} \quad (9)$$

In equation (9),  $\varepsilon$  is the load;  $\beta$  is the distance between the left and right loading points;  $A_1$  is the deflection in Z direction;  $A_2$  is the deflection in the negative Z direction (Deich et al., 2021).

As with the analysis of bending stiffness, three working conditions are considered for torsional stiffness analysis. The specific working conditions are as follows:

- The first working condition: concentrated force acts on the front lifting lug  
Apply a concentrated force of 3,000 N in the opposite Z direction at the front lifting lug, the value of  $\beta$  is 1,066, the deformation of the aluminium alloy frame is obtained, and the torsional stiffness analysis (Farsadi et al., 2021) is performed on it.
- The second working condition: concentrated force acts on the rear lifting lug  
Apply a concentrated force of 3,000 N in the opposite Z direction at the rear lifting lug, the value of  $\beta$  is 1,066, the deformation of the aluminium alloy frame is obtained, and the torsional stiffness analysis is performed on it.
- The third working condition: concentrated force acts on the support between them  
Apply 3,000 N and Z-direction opposite concentrated force on the support between the two, the value of  $\beta$  is 1,066, the deformation of the aluminium alloy frame is obtained, and the torsional stiffness analysis (Li et al., 2022) is performed on it.

### 3 Test

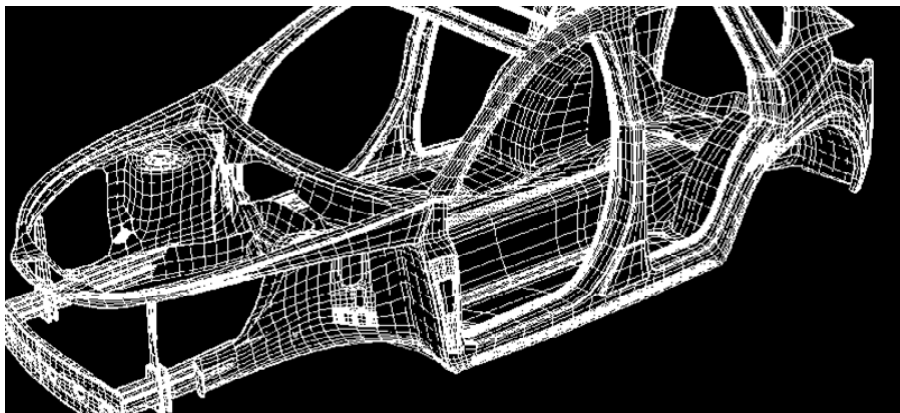
#### 3.1 Test vehicle

The vehicle under test is a new energy vehicle made of aluminium alloy frame. The final construction results of its finite element model are shown in Figure 10.

Add loads to the model, and perform bending stiffness analysis and torsional stiffness analysis.

#### 3.2 Bending stiffness analysis results

For the design method, in order to further investigate the overall bending deformation of the aluminium alloy frame, select multiple assessment points, record the deformation along the Z direction and the X coordinate value, draw a table, and observe the continuity of the aluminium alloy frame deformation. The absence of obvious mutation indicates that the whole frame has no structural problems caused by the design structure.

**Figure 10** Final construction results of finite element model

The selection of assessment points is to select one assessment point at the lower part of the frame threshold and the lower part of the longitudinal beam every 300 mm, a total of 36 assessment points are selected.

**Table 6** Record under the first working condition

<i>S/N</i>	<i>X coordinate (mm)</i>	<i>Average Z-direction deformation value of assessment point (mm)</i>		
		<i>Front side member</i>	<i>Threshold</i>	<i>Rear side member</i>
1	79.32	-0.0046	-	-
2	376.20	-0.2684	-	-
3	695.20	-0.7652	-	-
4	1,025.01	-1.1574	-0.7586	-
5	1,157.24	-	-0.9562	-
6	1,652.01	-	-0.8541	-1.5321
7	2,054.20	-	-	-1.1587
8	2,351.20	-	-	-0.6582
9	2,953.21	-	-	-0.0865
10	3,142.21	-	-	0.1853
11	3,598.63	-	-	0.4625
12	3,698.54	-	-	0.5685

The deformation along Z direction and X coordinate value records of each assessment point under the first working condition are shown in Table 6.

According to the results recorded in the above table, under the condition that the constraint is applied to the front lifting lug, there is no obvious mutation in the deformation of the selected assessment point along the Z direction, which indicates that the bending deformation of the aluminium alloy frame is continuous, and there is no structural problem caused by the design structure.

The deformation along Z direction and the record of X coordinate value of each assessment point under the second working condition are shown in Table 7.

**Table 7** Records under the second working condition

<i>S/N</i>	<i>X coordinate (mm)</i>	<i>Average Z-direction deformation value of assessment point (mm)</i>		
		<i>Front side member</i>	<i>Threshold</i>	<i>Rear side member</i>
1	79.32	-0.0484	-	-
2	376.20	-0.3865	-	-
3	695.20	-0.8012	-	-
4	1,025.01	-1.0147	-0.7365	-
5	1,157.24	-	-1.1420	-
6	1,652.01	-	-1.3652	-1.9785
7	2,054.20	-	-	-2.2654
8	2,351.20	-	-	-2.2698
9	2,953.21	-	-	-1.9854
10	3,142.21	-	-	-1.6524
11	3,598.63	-	-	-1.0257
12	3,698.54	-	-	-0.6254

According to the results recorded in the table above, under the condition that the constraint is applied to the rear lifting lug, there is no obvious mutation in the deformation of the selected assessment point along the Z direction, which indicates that the bending deformation of the aluminium alloy frame also has continuity, and there is no structural problem caused by the design structure.

The deformation along Z direction and the record of X coordinate value of each assessment point under the third working condition are shown in Table 8.

According to the results recorded in the table above, when the constraint is applied to the support between the two, there is no obvious mutation in the deformation of the selected assessment point along the Z direction, which indicates that the bending deformation of the aluminium alloy frame also has continuity, and it comprehensively indicates that the experimental aluminium alloy vehicle technology does not have structural problems caused by the design structure.

After the load is added, under the first working condition, the calculation result of the bending stiffness value of the experimental new energy vehicle is as follows:

$$G = \frac{4,000}{48} \times \frac{2.6525^3}{315e^{-3}} = 7.2652e + 004 (N \cdot m^2) \quad (10)$$

Under the second working condition, the calculation result of bending stiffness value is as follows:

$$G = \frac{4,000}{48} \times \frac{3.4625^3}{2.6851e^{-3}} = 3.6524e + 007 (N \cdot m^2) \quad (11)$$

Under the third working condition, the calculation result of bending stiffness value is as follows:

$$G = \frac{4,000}{48} \times \frac{2.8562^3}{1.6581e^{-3}} = 4.852e + 007 (N \cdot m^2) \quad (12)$$

Under the three working conditions, the bending stiffness of the aluminium alloy frame is high, indicating that the bending stiffness of the aluminium alloy frame is sufficient.

**Table 8** Record under the third working condition

S/N	X coordinate (mm)	Average Z-direction deformation value of assessment point (mm)		
		Front side member	Threshold	Rear side member
1	79.32	-0.0458	-	-
2	376.20	-0.4562	-	-
3	695.20	-0.8654	-	-
4	1,025.01	-1.1458	-0.7254	-
5	1,157.24	-	-0.9865	-
6	1,652.01	-	-1.0258	-1.8652
7	2,054.20	-	-	-1.6541
8	2,351.20	-	-	-1.3625
9	2,953.21	-	-	-0.8754
10	3,142.21	-	-	-0.4629
11	3,598.63	-	-	-0.0254
12	3,698.54	-	-	0.1985

In the test, the frame stiffness analysis method based on Hyperworks and the frame stiffness analysis method based on tube combined structure and finite element calculation plate are used as the comparison method to jointly test the bending stiffness calculation, and compare with the actual value to calculate the bending stiffness analysis error. Methods 1 and 2 are used to represent the above two comparison methods in the test.

The comparison test results are shown in Table 9.

**Table 9** Comparison test results

Method	Bending stiffness analysis error under condition 1 ( $N \cdot m^2$ )	Bending stiffness analysis error under condition 2 ( $N \cdot m^2$ )	Bending stiffness analysis error under condition 3 ( $N \cdot m^2$ )
Design method	2e+0.02	2e+0.01	3e+0.05
Method 1	5e+0.06	6e+0.02	6e+0.08
Method 2	6e+0.05	5e+0.03	7e+0.09

According to the test results in Table 9, the bending stiffness analysis error of the design method under three working conditions is less than that of the two comparison methods, which indicates that the bending stiffness analysis accuracy of the design method is higher.

### 3.3 Results of torsional stiffness analysis

In order to further investigate the overall bending deformation in the torsional stiffness analysis of the aluminium alloy frame, record the deformation along the Z direction and the X coordinate value of the assessment point in the upper section, draw a table, and

observe the continuity of the deformation of the aluminium alloy frame. The absence of obvious mutation indicates that the whole frame has no structural problems caused by the design structure.

The deformation along Z direction and X coordinate value records of each assessment point under the first working condition are shown in Table 10.

**Table 10** Record under the first working condition

<i>S/N</i>	<i>X coordinate (mm)</i>	<i>Average Z-direction deformation value of assessment point (mm)</i>		
		<i>Front side member</i>	<i>Threshold</i>	<i>Rear side member</i>
1	79.32	0.2652	-	-
2	376.20	0.2754	-	-
3	695.20	0.5976	-	-
4	1,025.01	2.1547	2.9685	-
5	1,157.24	-	4.5214	-
6	1,652.01	-	5.8965	4.6587
7	2,054.20	-	-	6.3587
8	2,351.20	-	-	7.5487
9	2,953.21	-	-	8.6327
10	3,142.21	-	-	9.5487
11	3,598.63	-	-	10.2514
12	3,698.54	-	-	11.6585

According to the results recorded in the above table, under the first working condition, there is no obvious sudden change in the torsional deformation of the selected assessment point along the Z direction, which indicates that the torsional deformation of the aluminium alloy frame has continuity, that is, there is no structural problem caused by the design structure of the frame.

**Table 11** Record under the second working condition

<i>S/N</i>	<i>X coordinate (mm)</i>	<i>Average Z-direction deformation value of assessment point (mm)</i>		
		<i>Front side member</i>	<i>threshold</i>	<i>Rear side member</i>
1	79.32	0.2658	-	-
2	376.20	0.2985	-	-
3	695.20	0.8477	-	-
4	1,025.01	1.9845	2.8745	-
5	1,157.24	-	3.5854	-
6	1,652.01	-	4.2457	5.3641
7	2,054.20	-	-	6.7450
8	2,351.20	-	-	7.9687
9	2,953.21	-	-	8.0214
10	3,142.21	-	-	9.3201
11	3,598.63	-	-	10.5471
12	3,698.54	-	-	11.5785

The deformation along Z direction and the record of X coordinate value of each assessment point under the second working condition are shown in Table 11.

The results recorded in the above table show that under the second working condition, there is no obvious mutation in the deformation of the selected assessment point along the Z direction, indicating that the torsional deformation of the aluminium alloy frame also has continuity, and the aluminium alloy frame does not have structural problems caused by the design structure.

The deformation along Z direction and the record of X coordinate value of each assessment point under the third working condition are shown in Table 12.

**Table 12** Record under the third working condition

S/N	X coordinate (mm)	Average Z-direction deformation value of assessment point (mm)		
		Front side member	threshold	Rear side member
1	79.32	0.2265	-	-
2	376.20	0.2658	-	-
3	695.20	0.8562	-	-
4	1025.01	1.9562	2.9865	-
5	1157.24	-	3.6587	-
6	1652.01	-	4.5874	4.6254
7	2054.20	-	-	6.5874
8	2351.20	-	-	7.5847
9	2953.21	-	-	8.4571
10	3142.21	-	-	9.3244
11	3598.63	-	-	9.9854
12	3698.54	-	-	10.2154

The results recorded in the above table show that under the third working condition, there is also no obvious mutation in the deformation of the selected assessment point along the Z direction, indicating that the torsional deformation of the aluminium alloy frame also has continuity, which more comprehensively indicates that the experimental aluminium alloy vehicle technology does not have structural problems caused by the design structure.

Under the first working condition, the calculation result of torsional stiffness value is as follows:

$$O = \frac{3,000 \times 1.2587 \times \pi}{\arcsin\left(\frac{3.9854 + 4.6985}{1.2587}\right)} \times 180 = 7,548 \text{ (N} \cdot \text{m/}^\circ\text{)} \quad (13)$$

Under the second working condition, the calculation result of torsional stiffness value is as follows:

$$O = \frac{3,000 \times 1.2587 \times \pi}{\arcsin\left(\frac{6.5124 + 5.5687}{1.2587}\right)} \times 180 = 5,874 \text{ (N} \cdot \text{m/}^\circ\text{)} \quad (14)$$

Under the third working condition, the calculation result of torsional stiffness value is as follows:

$$O = \frac{3,000 \times 1.2587 \times \pi}{\arcsin\left(\frac{4.6985 + 4.5741}{1.2587}\right) \times 180} = 6,985 \text{ (N} \cdot \text{m/}^\circ\text{)} \quad (15)$$

According to the calculation results, under the three working conditions, the torsional stiffness of the aluminium alloy frame is high, indicating that the torsional stiffness of the aluminium alloy frame is sufficient.

The comparative test results of the three methods are shown in Table 13.

**Table 13** Comparison test results

<i>Method</i>	<i>Torsional stiffness analysis error under condition 1 (N·m/°)</i>	<i>Torsional stiffness analysis error under condition 2 (N·m/°)</i>	<i>Torsional stiffness analysis error under condition 3 (N·m/°)</i>
Design method	26	22	28
Method 1	32	30	56
Method 2	41	47	57

The test results in the above table show that the torsional stiffness analysis error of the design method under three working conditions is the smallest, while the torsional stiffness analysis error of methods 1 and 2 is larger, which indicates that the bending stiffness analysis accuracy of the design method is higher.

## 4 Conclusions

The purpose of this study is to design a stiffness analysis method of automobile aluminium alloy frame based on the finite element model to meet the requirements of lightweight design of new energy vehicles. By only considering the main structural components and properly simplifying their structures, the calculation efficiency and accuracy requirements are improved when building the finite element model. By building the model of each component and assembling it into an integral frame model, incorporating it into the suspension system and dividing the model grid, the additional mass and assembly mass are simplified as a concentrated load applied on the supporting points, and the frame's own mass is simplified as a uniformly distributed load applied on nodes and elements. Through the analysis of bending stiffness and torsional stiffness, the stiffness characteristics of aluminium alloy frame are obtained. The test results show that through this design method, the bending stiffness and torsional stiffness analysis of the aluminium alloy frame can be achieved, and the error is very small, the lowest is  $2e+0.01 \text{ N} \cdot \text{m}^2$  and  $22 \text{ N} \cdot \text{m/}^\circ$ . It shows that this method can help engineers better understand the stiffness characteristics of aluminium alloy frames, and provide a basis for optimal design.

## Acknowledgements

This work was funded by Research and Practice Project of Teaching Reform of Local Universities in Zhengzhou (ZZJG-A1016).

## References

- Ci, S., Jiang, R., Liu, D. and Chen, H. (2022) 'Lightweight design of CFRP bicycle frames', *Journal of Machine Design*, Vol. 39, No. 2, pp.13–17.
- De, A.F.Y., Portelles, J., Lopez-Noda, R., Fuentes, J., Hmok, H. and Siqueiros, J.M. (2021) 'An analysis of the ferroelastic transition in  $\text{Pb}(\text{Zr}_{0.53}\text{Ti}_{0.47})\text{O}_{3-\delta}$  through the elastic stiffness constant', *Phase Transitions*, Vol. 94, No. 5, pp.308–316.
- Deich, T., Storch, M., Kai, S. and Bund, A. (2021) 'Effects of module stiffness and initial compression on lithium-ion cell aging', *Journal of Power Sources*, Vol. 506, No. 15, pp.230–236.
- De-La-Colina, J., Valdes-Gonzalez, J. and Manzanarez Morones, F. (2021) 'Accidental torsion within the frame of nonlinear dynamic analysis using code accidental eccentricities and Monte Carlo simulations', *Engineering Structures*, Vol. 248, No. 1, pp.1131–1139.
- Depalo, F., Wang, S., Xu, S., Soares, C.G., Yang, S.H. and Ringsberg, J.W. (2022) 'Effects of dynamic axial stiffness of elastic moorings for a wave energy converter', *Ocean Engineering*, Vol. 251, No. 1, pp.1111–1118.
- Doornebosch, L.M., Abbink, D.A. and Peternel, L. (2021) 'Analysis of coupling effect in human-commanded stiffness during bilateral tele-impedance', *IEEE Transactions on Robotics: A Publication of the IEEE Robotics and Automation Society*, Vol. 37, No. 4, pp.1282–1297.
- Farsadi, T., Asadi, D. and Kurtaran, H. (2021) 'Fundamental frequency optimization of variable stiffness composite skew plates', *Acta Mechanica*, Vol. 232, No. 2, pp.555–573.
- Goswami, M., Ghorai, S.K., Sharma, S., Chakraborty, G. and Chattopadhyay, S. (2021) 'Nonlinear fracture assessment and nanomechanical deformation of elastomeric composites: development of finite element model and experimental validation', *Polymer Composites*, Vol. 42, No. 7, pp.3572–3592.
- Hajibabazadeh, S., Aghjeh, M.R. and Mazidi, M.M. (2021) 'Stiffness-toughness balance in PP/EPDM/SiO<sub>2</sub> ternary blend-nanocomposites: The role of microstructural evolution', *Journal of Composite Materials*, Vol. 55, No. 2, pp.265–275.
- Jaafari, C., Grange, S., Bertrand, D., Georgin, J.F., Delhomme, F. and Tardif, N. (2022) 'Multifiber finite element model based on enhanced concrete constitutive law to account for the effects of early age damage on the seismic response of RC structures', *Engineering Structures*, Vol. 256, No. 11, pp.138–146.
- Li, C., Lin, J., Qian, Y. and Dai, H. (2022) 'Lightweight design of a car body in white based on finite element analysis', *Computer Simulation*, Vol. 39, No. 9, pp.144–149.
- Li, H., Chen, W., Pham, T.M. and Hao, H. (2021) 'Analytical and numerical studies on impact force profile of RC beam under drop weight impact', *International Journal of Impact Engineering*, Vol. 147, No. 26, pp.1037–1045.
- Liu, X., Zhao, X. and Liu, X. (2022) 'A highly accurate spectral dynamic stiffness method for efficient broadband modal and dynamic response analysis of membranes assemblies with arbitrary boundary conditions', *Computers & Structures*, Vol. 267, No. 15, pp.106–113.
- Saidou, A., Gauron, O., Busson, A. and Paultre, P. (2021) 'High-order finite element model of bridge rubber bearings for the prediction of buckling and shear failure', *Engineering Structures*, Vol. 240, No. 1, pp.112–116.

- Sayed, H. and El-Sayed, T.A. (2022) 'Nonlinear dynamics and bifurcation analysis of journal bearings based on second order stiffness and damping coefficients', *International Journal of Non-Linear Mechanics*, Vol. 142, No. 55, pp.1039–1048.
- Sharma, T., Murari, V. and Shukla, K.K. (2021) 'Effects of aerofoil, twist and wind speed on the structural response of 1D finite element model of wind turbine blade', *Journal of Structural Engineering*, Vol. 48, No. 2, pp.131–145.
- Stefenon, S.F., Seman, L.O., Pavan, B.A., Ovejero, R.G. and Leithardt, V.R.Q. (2022) 'Optimal design of electrical power distribution grid spacers using finite element method', *IET Generation, Transmission & Distribution*, Vol. 16, No. 9, pp.1865–1876.
- Witkowski, K., Kudra, G., Wasilewski, G. and Awrejcewicz, J. (2022) 'Mathematical modelling, numerical and experimental analysis of one-degree-of-freedom oscillator with Duffing-type stiffness', *International Journal of Non-Linear Mechanics*, Vol. 138, No. 56, pp.1038–1045.
- Zhan, J., Wang, Y., Zhang, F., An, Y. and Liu, K. (2022) 'Scour depth evaluation of highway bridge piers using vibration measurements and finite element model updating', *Engineering Structures*, Vol. 253, No. 15, pp.113–118.